Label-free Biosensor Array Based on Silicon-on-Insulator Ring Resonators Addressed Using a WDM Approach

Xu, D. -X.; Vachon, M.; Densmore, A.; Ma, R.; Delâge, A.; Janz, S.; Lapointe, J.; Li, Y.; Lopinski, G.; Zhang, D.; Liu, Q. Y.; Cheben, P.; Schmid, J. H.

Publisher's version / Version de l'éditeur:
https://doi.org/10.1364/OL.35.002771
Optics Letters, 35, 16, pp. 2771-2773, 2010-08-01

Label-free biosensor array based on silicon-on-insulator ring resonators addressed using a WDM approach

D.-X. Xu,[1,*] M. Vachon,[1] A. Densmore,[1] R. Ma,[1] A. Delâge,[1] S. Janz,[1] J. Lapointe,[1] Y. Li,[2] G. Lopinski,[2] D. Zhang,[3] Q. Y. Liu,[3] P. Cheben,[1] and J. H. Schmid[1]

[1]*Institute for Microstructural Sciences, National Research Council Canada, Ottawa, Ontario, Canada, K1A 0R6*

[2]*Steacie Institute for Molecular Sciences, National Research Council Canada, Ottawa, Ontario, Canada, K1A 0R6*

[3]*Institute for Biological Sciences, National Research Council Canada, Ottawa, Ontario, Canada, K1A 0R6*

**Corresponding author: Danxia.Xu@Nrc-cnrc.gc.ca*

Received June 4, 2010; accepted June 24, 2010;
posted July 28, 2010 (Doc. ID 129622); published August 13, 2010

We report a silicon-on-insulator ring resonator biosensor array with one output port, using wavelength division multiplexing as the addressing scheme. With the use of on-chip referencing for environmental drift cancellation, simultaneous monitoring of multiplexed molecular bindings is demonstrated, with a resolution of 0.3 pg/mm^2 (40 ag of total mass) for protein concentrations over 4 orders of magnitude down to 20 pM. Reactions are measured over time periods as long as 3 h with high stability.

OCIS codes: 130.3120, 230.5750, 130.6010, 120.0120.

Monitoring of molecular interactions provides critical information for medical diagnosis, drug development, environmental protection, and security. The presence and concentration of target molecules, as well as receptor-target binding affinity and kinetics, can be measured by monitoring the binding between molecules of interest, e.g., proteins, biomarkers, and complementary DNA segments. Because of the complex nature of most biological interactions, sensor arrays capable of multiplexed measurements are often required. Miniaturization, low cost, and portability are desirable attributes for such sensing systems.

Label-free evanescent field sensors made of silicon-on-insulator (SOI) photonic waveguides with submicrometer dimensions have seen rapid development in recent years [1–5]. Because of the high refractive index of silicon, the optical modal field is strongly localized near the waveguide surface, resulting in a high response to surface perturbations, particularly when operating in the TM mode [2]. Highly compact SOI sensor arrays are readily manufacturable using standard complementary metal-oxide semiconductor processing. The use of ring resonators further amplifies the sensor response, because the light circulating in the ring effectively interacts with the same molecules many times [2,6,7]. These properties make Si wire resonators one of the most promising sensor platforms.

Several groups have investigated sensor arrays with the sensing elements addressed using power splitting, where multiple outputs are captured with an imaging system [1,3,5]. Imaging systems are comparatively costly and have limited data acquisition speed [5] unless sophisticated instrumentation is employed [3]. Here we report a sensor array with ring resonators arranged in a series and coupled to a common access waveguide. Each resonator has a distinct set of resonances correlated with its ring size, and the resonance wavelength is used as the address for each ring using wavelength division multiplexing (WDM). The sensing signals for all the rings are captured using a single detector, allowing simple instrumentation. We demonstrate high uniformity between the sensing elements and present results of simultaneous monitoring of multiple antigen-antibody binding reactions in subnanomolar concentrations.

The sensor array configuration is shown in Fig. 1. A reference ring is used to cancel temperature-induced drift, and it is protected with a 2-μm-thick SU8 polymer cladding layer. Four sensing rings are exposed to the sensing medium by opening windows through the cladding [dotted lines in Fig. 1(a)]. A simple all-pass configuration is used, leading to a single output port. The add–drop sensor configuration has been explored previously [5]; however, that requires multiple output ports and an imaging setup for interrogation, similar to the power-splitting configuration. To separate the resonances from each sensor by ~1 nm, we choose the ring radii R as 20 (reference ring), 22, 24, 26, and 28 μm, respectively. The resonances used in the sensing experiments are not necessarily from the same resonance order, but the origin of the resonances can easily be identified by referring to their respective free spectral range (FSR $= \lambda_R^2/2\pi R n_g$), where λ_R is the resonance wavelength and n_g (~4.5) is the waveguide group index. Molecule adsorption induced effective index change Δn_{eff} is related to the resonance wavelength shift as $\Delta\lambda_R = \lambda_R \Delta n_{\text{eff}}/n_g$, independent of the ring size.

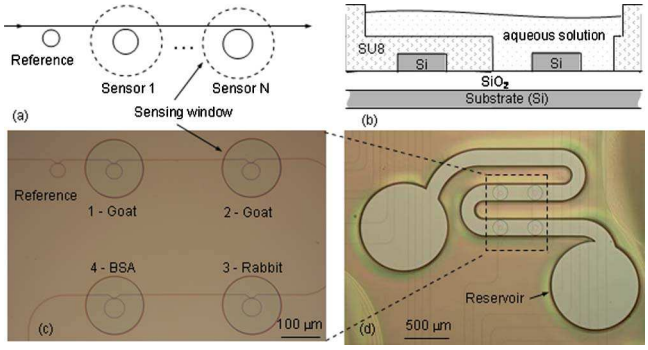

Fig. 1. (Color online) (a) Schematic of the WDM addressed ring sensor array, (b) corresponding cross section, (c) fabricated sensor array, and (d) sensor array with microfluidic channel.

The fabricated ring and access waveguides are 450 nm × 260 nm in cross section, designed to operate in the quasi-TM fundamental mode. A coupler of 3 μm long with a gap of 0.5 μm is employed in all the resonators, yielding a through-coupling strength of ~0.99 in the reference ring. The fabrication processes, inverse taper mode size converters used, microfluidics, and surface preparation procedures are identical to that reported previously [2]. The sensing windows in the 2-μm-thick SU8 cladding are 170 μm in diameter and placed on a 400 μm × 400 μm grid. A microfluidic channel was integrated on-chip using a second SU8 layer 50 μm in thickness [1]. The sensor surface was silanized in vapor phase by suspending the chip above liquid 3-aminopropylmethyldiethoxysilane in a sealed container for 20 min.

The transmission spectrum of the array under the sensing condition is shown in Fig. 2(a), where the labels indicate the resonators that the resonances originate from, based on their respective FSR. The assignments are also further verified during sensing. The reference ring shows a typical quality factor of $Q \sim 38,000$, while the sensing rings show a lower $Q \sim 25,000$. Analysis indicates that the decrease in Q is mainly due to the attenuation caused by the water absorption, while the change in the resonator coupling strength is small [8]. All sensing experiments were performed in a room environment without active temperature control, while the stage temperature was monitored. Solutions were delivered by drawing with a syringe pump at a rate of 2 mL/h. The laser was continuously scanned over a 10 nm wavelength range at 2 pm/step, and the light was coupled to the input waveguide via a lensed polarization maintaining fiber. A full spectrum takes ~6 s to acquire. The resonance positions were determined using a three-point parabolic fit to the intensity minima.

Sensor response was first calibrated using sucrose solutions of varying concentrations, and the as-measured data are shown in Fig. 2(b). Analyte solutions were delivered to all the sensors through a single fluidics channel [see Fig. 1(d)], in which the reference ring also resides (but covered with 2 μm thick SU8). The measured fluid index sensitivity is 135 nm/RIU (the fluid index change is 1.4×10^{-3} for 1% sucrose), independent of the ring size as predicted by theory. The resonance resolution is <0.3 pm, corresponding to a fluid index variation of $<2 \times 10^{-6}$, and the response variation between the four sensors is ±1 pm for an $\Delta\lambda_R$ of 95 pm. This excellent sensing uniformity indicates good dimensional and fluidic uniformities of the sensors. The reference ring λ_R blueshifted ~17 pm over the duration of the experiment (25 min). We found that this shift includes contributions from the temperature fluctuations and a slow drift, which we believe is related to the gradual water permeation into the SU8 cladding. The later contribution is a monotonic function of the fluid exposure time, and we have calibrated it separately with experiments under a stabilized temperature. Details of these procedures will be reported in a separate publication. Using the reference ring to cancel the temperature-induced fluctuations [9], the baseline [in deionized (DI) water] for all four sensors are maintained to $< \pm 2$ pm during the entire experiment.

To demonstrate multiplexed molecular binding, we use the interaction between antigen-antibody pairs, namely goat and antigoat immunoglobulin G (IgG) and rabbit and antirabbit IgG. After the initial silanization, receptor molecules goat and rabbit IgG were deposited on sensors 1–3 individually, and bovine serum albumin (BSA) was deposited on sensor 4 as a control, as labeled in Fig. 1(c), using a noncontact spotter. The spotting was performed at room temperature in 50% humidity [10], using solutions of 1 mg/mL in phosphate buffered saline (PBS). The samples were then left to incubate for 1 h in the spotter and removed for storage at 4 °C in a dry environment. In testing molecular binding, BSA solution (1 mg/mL) was first flowed for 25 min to block unoccupied silane molecules, followed by a PBS rinse for ~15 min prior to introducing the antirabbit and antigoat IgG analyte. The response of sensor 3 (spotted with rabbit IgG) to antirabbit IgG of 0.02, 2, 20, and 200 nM concentrations is shown in Fig. 3. The initial response shows the characteristic linear behavior. The apparent binding rate is shown in Fig. 3(b) as a function of the concentration over a dynamic range extending 4 orders of magnitude, for both the antirabbit–rabbit and antigoat–goat IgG bindings. The error bars are based on data from the different sensor elements and repeated experiments. By taking into account the effects of mass transport [2,11], molecular binding kinetic information can be obtained for even very dilute solutions.

Binding reactions to consecutive analyte injections are shown in Fig. 4, after background drift corrections using the reference ring. After the initial BSA and PBS flow, antirabbit and antigoat IgG solutions (2 nM) were injected, separated by PBS rinsing steps. Sensor 3 showed a strong binding of the rabbit IgG receptor to the antirabbit IgG in solution, with $\Delta\lambda_R \sim 150$ pm. As expected,

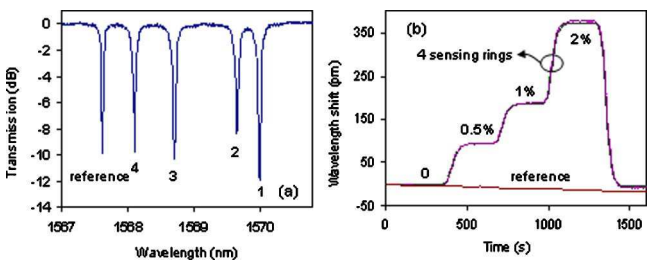

Fig. 2. (Color online) (a) Transmission spectrum of the ring sensor array. The labels indicate the resonators that the resonances originate from, as marked in Figs. 1(c) and 1(b). (b) As-measured wavelength shift of the sensors in 0.5%, 1%, and 2% sucrose solutions relative to DI water.

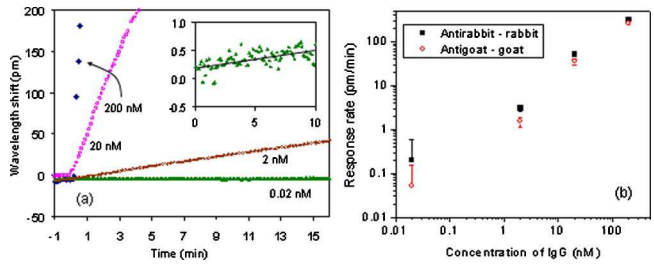

Fig. 3. (Color online) (a) Wavelength shift of sensor 3 (spotted with rabbit IgG) upon exposure to varying concentrations of antirabbit IgG. Inset, a close up of the response to 0.02 nM IgG. (b) Response rate between complementary protein pairs at varying IgG concentrations.

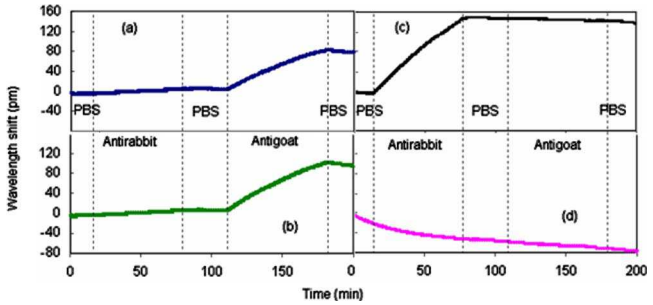

Fig. 4. (Color online) (a) Corrected wavelength shift of the sensor array in response to consecutively injected 2 nM IgG solutions. (a) and (b) sensor 1 and 2—goat IgG spotted, (c) sensor 3—rabbit IgG spotted, and (d) sensor 4—BSA spotted.

sensors 1 and 2 functionalized with goat IgG demonstrated a much smaller response to the antirabbit IgG ($\Delta\lambda_R \sim 10$ pm over 80 min), corresponding to a 15:1 binding selectivity. When antigoat IgG solution was introduced at 110 min, sensors 1 and 2 showed a large response, reaching 77 pm and 94 pm, respectively, while the response of sensor 3 was minimal. Because the intrinsic sensing response is highly uniform as demonstrated with sucrose solutions, the difference in protein response is most likely caused by receptor coverage nonuniformity due to variable drying. The response of the BSA spotted sensor 4 showed a continuous decrease in λ_R, and this behavior was consistently observed in these experiments with different IgG concentrations. We speculate that this drift is caused by the removal of loosely bound BSA molecules deposited by spotting.

Based on the experiment using 200 nM IgG solutions, a saturated $\Delta\lambda_R$ of 1200 pm corresponds to the binding of a full monolayer. Separate calibration using ellipsometry estimates a surface mass coverage of 1.2 ng/mm^2 [1,12]. The measured wavelength resolution of 0.3 pm therefore corresponds to a resolvable surface coverage of 0.3 pg/mm^2, which is approximately 0.03% of a saturated molecular monolayer, or a total mass of 40 ag for a ring sensor with $R \sim 20$ μm. These values represent a significant advance over existing commercial systems.

In summary, we have presented an SOI ring resonator serial array for label-free biosensing applications. The array consists of one reference ring and four sensing rings of different radii, with one output and addressed using WDM for multiplexed measurements. This configuration may be extended to include more sensors, provided the adsorption induced resonance shifts are considerably smaller than the ring FSRs. The array is integrated with an on-chip fluidic channel, and receptor molecules are deposited in individual sensors using a noncontact spotter. The sensing response exhibits high sensitivity and excellent uniformity. Using the reference ring to remove spurious environmental drifts, highly stable sensing signals are obtained. Multiplexed binding between complementary and mismatched IgG protein pairs are monitored simultaneously, down to a concentration of 20 pM, demonstrating a resolvable mass of 40 ag and a selectivity of >15:1. The simplicity of this array configuration makes it particularly suitable for small sensing systems with a low channel count. This design may also be combined with power splitting to generate large arrays.

References

1. A. Densmore, M. Vachon, D.-X. Xu, S. Janz, R. Ma, Y.-H. Li, G. Lopinski, A. Delâge, J. Lapointe, C. C. Luebbert, Q. Y. Liu, P. Cheben, and J. H. Schmid, Opt. Lett. **34**, 3598 (2009).
2. D.-X. Xu, A. Densmore, A. Delâge, P. Waldron, R. McKinnon, S. Janz, J. Lapointe, G. Lopinski, T. Mischki, E. Post, P. Cheben, and J. H. Schmid, Opt. Express **16**, 15137 (2008).
3. A. L. Washburn, L. C. Gunn, and R. C. Bailey, Anal. Chem. **81**, 9499 (2009).
4. N. Skivesen, A. Tu, M. Kristensen, L. Frandsen, and P. Borel, Opt. Express **15**, 3169 (2007).
5. K. De Vos, J. Girones, T. Claes, Y. De Koninck, S. Popelka, E. Schacht, R. Baets, and P. Bienstman, IEEE Photonics J. **1**, 225 (2009).
6. N. Jokerst, M. Royal, S. Palit, L. Luan, S. Dhar, and T. Tyler, J. Biophoton. **2**, 212 (2009).
7. J. H. Schmid, W. Sinclair, J. García, S. Janz, J. Lapointe, D. Poitras, Y. Li, T. Mischki, G. Lopinski, P. Cheben, A. Delâge, A. Densmore, P. Waldron, and D.-X. Xu, Opt. Express **17**, 18371 (2009).
8. W. R. McKinnon, D.-X. Xu, C. Storey, E. Post, A. Densmore, A. Delâge, P. Waldron, J. H. Schmid, and S. Janz, Opt. Express **17**, 18971 (2009).
9. D.-X. Xu, A. Densmore, R. Ma, J. H. Schmid, M. Vachon, J. Lapointe, S. Janz, E. Post, A. Delâge, and P. Cheben, in *6th IEEE International Conference on Group IV Photonics* (IEEE, 2009), WC3, pp. 34–36.
10. E. Olle, J. Messamore, M. Deogracias, S. McClintock, T. Anderson, and K. Johnson, Exp. Mol. Pathol. **79**, 206 (2005).
11. J. Stepánek, H. Vaisocherová, and M. Piliarik, eds., *Surface Plasmon Resonance Based Sensors* (Springer, 2006), Vol. 4, pp. 69–91.
12. H. Elwing, Biomaterials **19**, 397 (1998).